

PBX1-directed stem cell transcriptional program drives tumor progression in myeloproliferative neoplasm

Sharon Muggeo,^{1,2,10,14} Laura Crisafulli,^{1,2,14} Paolo Uva,^{3,11} Elena Fontana,^{1,2} Marta Ubezio,⁴ Emanuela Morengi,⁵ Federico Simone Colombo,^{6,12} Rosita Rigoni,^{1,2} Clelia Peano,^{1,7,13} Paolo Vezzoni,^{1,2} Matteo Giovanni Della Porta,^{4,8} Anna Villa,^{1,9} and Francesca Ficara^{1,2,*}

¹UOS Milan Unit, Istituto di Ricerca Genetica e Biomedica (IRGB), CNR, Milan, Italy

²Human Genome and Biomedical Technologies Unit, IRCCS Humanitas Research Hospital, via Manzoni 56, Rozzano, Milan 20089, Italy

³CRS4, Science and Technology Park Polaris, Pula (CA), Italy

⁴Department of Oncology and Hematology, IRCCS Humanitas Research Hospital, via Manzoni 56, Rozzano, 20089 Milan, Italy

⁵Biostatistics Unit, IRCCS Humanitas Research Hospital, via Manzoni 56, Rozzano, Milan, Italy

⁶Flow Cytometry Core, IRCCS Humanitas Research Hospital, via Manzoni 56, Rozzano, 20089 Milan, Italy

⁷Genomic Unit, IRCCS Humanitas Research Hospital, via Manzoni 56, Rozzano, 20089 Milan, Italy

⁸Department of Biomedical Sciences, Humanitas University, Via Rita Levi Montalcini 4, Pieve Emanuele, 20090 Milan, Italy

⁹San Raffaele Telethon Institute for Gene Therapy (SR-TIGET), IRCCS San Raffaele Scientific Institute, Milan, Italy

¹⁰Present address: Stem Cell and Neurogenesis Unit, Division of Neuroscience, San Raffaele Scientific Institute, Milan, Italy

¹¹Present address: IRCCS G. Gaslini, 16147 Genoa, Italy

¹²Present address: Servizio di Citofluorimetria, Fondazione IRCCS Ca' Granda Ospedale Maggiore Policlinico, Milan, Italy

¹³Present address: Human Technopole, Via Rita Levi Montalcini 1, Milan, Italy

¹⁴These authors contributed equally

*Correspondence: francesca.ficara@humanitasresearch.it

<https://doi.org/10.1016/j.stemcr.2021.09.016>

SUMMARY

PBX1 regulates the balance between self-renewal and differentiation of hematopoietic stem cells and maintains proto-oncogenic transcriptional pathways in early progenitors. Its increased expression was found in myeloproliferative neoplasm (MPN) patients bearing the *JAK2*^{V617F} mutation. To investigate if PBX1 contributes to MPN, and to explore its potential as therapeutic target, we generated the JP mouse strain, in which the human *JAK2* mutation is induced in the absence of PBX1. Typical MPN features, such as thrombocytopenia and granulocytosis, did not develop without PBX1, while erythrocytosis, initially displayed by JP mice, gradually resolved over time; splenic myeloid metaplasia and *in vitro* cytokine independent growth were absent upon PBX1 inactivation. The aberrant transcriptome in stem/progenitor cells from the MPN model was reverted by the absence of PBX1, demonstrating that PBX1 controls part of the molecular pathways deregulated by the *JAK2*^{V617F} mutation. Modulation of the PBX1-driven transcriptional program might represent a novel therapeutic approach.

INTRODUCTION

Myeloproliferative neoplasms are heterogeneous diseases in which platelets and/or mature blood cells of the myelo-erythroid lineage are produced in large excess (Tefferi, 2016) and that can ultimately evolve into acute leukemia. The three main MPN subtypes are polycythemia vera (PV), essential thrombocythemia (ET), and primary myelofibrosis (PMF), often characterized by the somatic V617F mutation in the *JAK2* tyrosine kinase, which renders it constitutively active irrespective of cytokine stimulation. *JAK2*^{V617F} is considered a phenotypic driver mutation (Nangalia and Green, 2017), although it is not sufficient to explain the heterogeneity of these diseases. Despite MPN being due to hyperproduction of mature cells, *JAK2*^{V617F} is present in patients' hematopoietic stem cells (HSCs), suggesting that they are targets of the initiating genetic lesion (Mead and Mullally, 2017).

PBX1 is a homeodomain transcription factor that binds DNA as a complex with HOX and MEIS/PREP proteins (Longobardi et al., 2014; Moens and Selleri, 2006), and that

is involved in chromosomal translocations leading to pediatric pre-B acute lymphoblastic leukemia (Nourse et al., 1990). PBX1 is one of the key factors regulating the balance between self-renewal and differentiation in HSCs (Ficara et al., 2008). In addition, PBX1 acts in multipotent and common myeloid progenitors to preserve their pool by temporally restricting proliferation and myeloid differentiation, and to preserve lymphoid and erythroid potential (Ficara et al., 2013). Bioinformatics analysis of gene expression data and experimental evidence revealed that PBX1 maintains proto-oncogenic transcriptional pathways involved in solid tumors and in myelo-proliferative disorders (Ficara et al., 2013; Jung et al., 2016; Wei et al., 2018), conceivably by virtue of its role in inhibiting differentiation in multiple stages of the hematopoietic hierarchy. Indeed, *PBX1* copy number variation was found in a subset of MPN patients bearing *JAK2*^{V617F} mutation (Rice et al., 2011), and PBX1 is overexpressed in cluster of differentiation (CD) 34⁺ cells from PV patients (Berkofsky-Fessler et al., 2010). Moreover, *Pbx1* is downregulated in murine *Jak2*-deficient hematopoietic stem and progenitor cells (HSPCs) (Akada et al., 2014), suggesting that it is part of



**Table 1. Overlap between MPN and PBX1 signatures**

Study	Sorted cells	MPN subgroup	Gene set size (DE IN MPN)		Common with PBX1 signature (IC DE) ^a	p-value
Rice et al., 2011	PB granulocytes	PV, ET, PMF	UP:	766	52 (6.8%) ^b	2.6×10^{-9}
			DOWN:	454	5 (1.1%)	n.s.
Rampal et al., 2014	PB granulocytes	PV, ET, PMF	UP:	1608	94 (5.8%)	2.5×10^{-12}
			DOWN:	1606	16 (1.0%)	n.s.
Berkofsky-Fessler et al., 2010	BM CD34 ⁺	PV	UP:	49	12 (24.5%)	6.7×10^{-9}
			DOWN:	243	9 (3.7%)	0.0027
Guglielmelli et al., 2007	PB CD34 ⁺	PMF	UP:	185	25 (13.5%)	6.2×10^{-11}
			DOWN:	211	12 (5.7%)	9.6×10^{-6}

The PBX1 signature and the lists of common genes are included in [Tables S1](#) and [S3](#), respectively. IC, inversely correlated. n.s., not significant.

^aOverlap analysis refers to common and anti-correlated genes.

^bPercentage values in brackets is calculated on the corresponding MPN DE values.

JAK2 signaling, and its overexpression in *JAK2*-mutant HSCs contributes to sustaining an MPN phenotype *in vivo* (Shepherd et al., 2018). Therefore, we reasoned that an aberrant expression of PBX1 or of its targets might contribute to the establishment or the maintenance of myeloid pre-leukemic clones. To test this hypothesis, we generated a new mouse model by crossing a *Pbx1*-conditional knockout (*Pbx1*-cKO) (Ficara et al., 2008) with a known *JAK2*^{V617F} MPN model (*JAK2*^{V617F}-conditional knockin [*JAK2*-cKI], developed by Li et al., 2010). In *JAK2*-cKI/*Pbx1*-cKO mice (hereafter JP for brevity), we can simultaneously activate the human *JAK2* mutation and delete *Pbx1* in the adult HSC compartment upon polyinosinic-polycytidylic acid (pIpC) administration.

We demonstrate that PBX1 plays a crucial role in MPN, since its absence modified the course of MPN: our model showed initial *JAK2*-dependent erythrocytosis that progressively disappeared after conditional PBX1 deletion, and the absence of other MPN-like symptoms. **Therefore, PBX1 is essential for the maintenance of the malignant clone, rather than for initiating the disease.** We also show that, despite the blood pathology in MPN being mediated by differentiated cells, transcriptional changes already occur at the level of early progenitors. RNA sequencing (RNA-seq) data confirmed that PBX1 in HSPCs controls part of the molecular pathways deregulated by the *JAK2*^{V617F} mutation.

RESULTS

Pbx1 controls part of the MPN signature

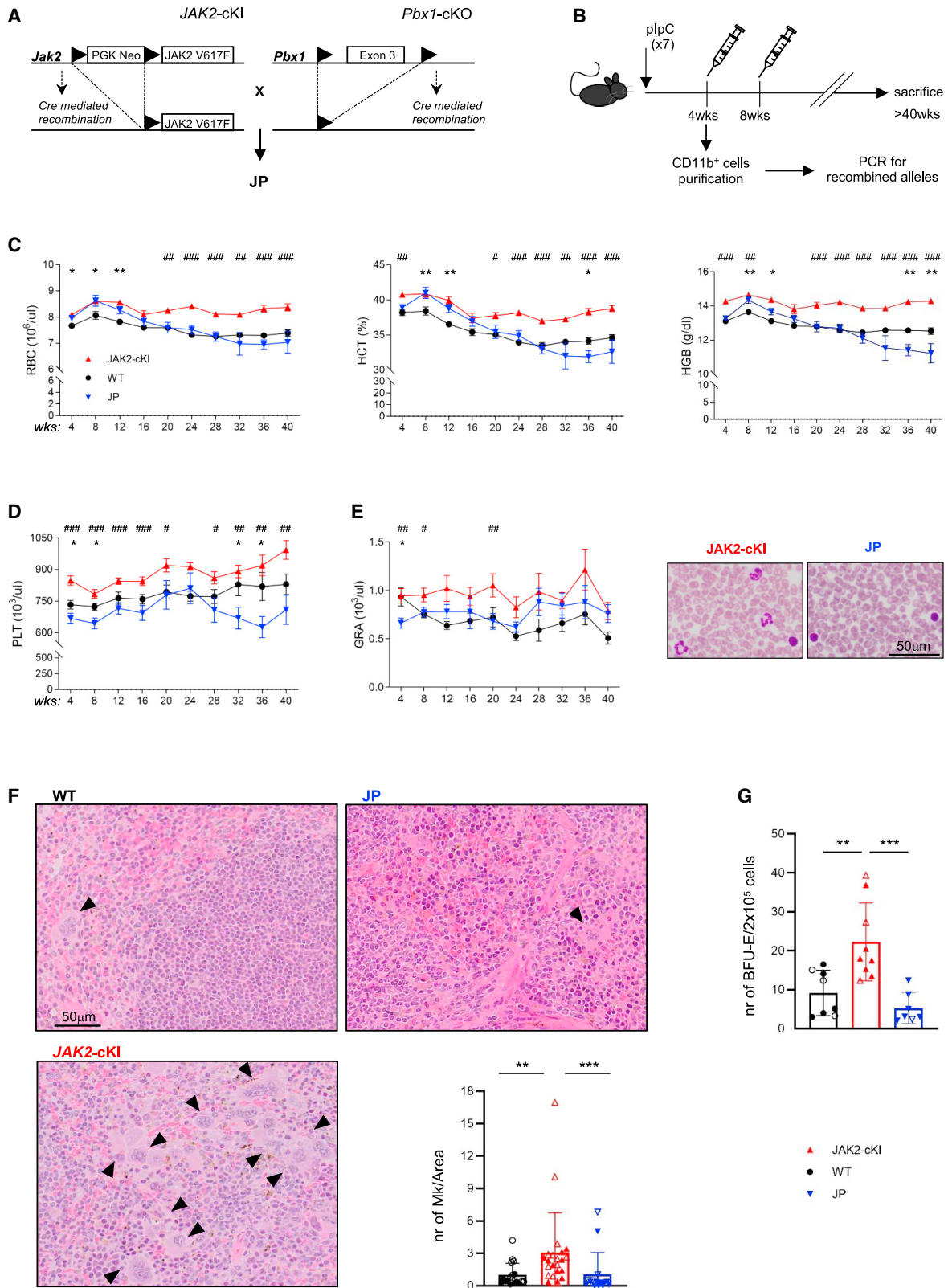
We first interrogated the literature to find some *in silico* evidence of a possible involvement of PBX1 in human MPN. We retrieved a human MPN expression profile from four

previously published studies (Berkofsky-Fessler et al., 2010; Guglielmelli et al., 2007; Rampal et al., 2014; Rice et al., 2011), in which data have been obtained either from granulocytes of several PV, PMF, or ET patients, or from CD34⁺ cells of PV or PMF patients. There is a considerable overlap between the two studies with similar disease subgroup and cell sources (Figures S1A and S1B and Table 1). A PBX1-dependent transcriptional program was obtained from our previously published profiles of *Pbx1*-cKO HSCs and progenitors (Table S1). When we compared the PBX1 and each MPN signature, we found that a significant proportion of the genes downregulated in the absence of PBX1 are upregulated in MPN patients (Table 1, up to 24.5% overlap). Similarly, a significant proportion of the genes upregulated in the absence of PBX1 are downregulated in CD34⁺ cells of PV and PMF patients. This is in accordance with the hypothesis that PBX1, directly or indirectly, may control part of the MPN signature. In addition, in the bone marrow (BM) CD34⁻ fraction of five *JAK2*^{V617F} patients analyzed, we found a tendency to a higher expression of PBX1 compared with healthy donors, despite PBX1 being a stem cell transcription factor that is expected to be expressed mainly in the CD34⁺ fraction (Figure S1C).

These data provided a strong rationale for asking if MPN course might be modified by acting on PBX1 or on its molecular signature.

PBX1 expression in *JAK2*^{V617F} HSCs is necessary to sustain MPN

To explore the role of PBX1 in MPN, we undertook a classic genetic approach, by crossing a previously described *JAK2*^{V617F} inducible knockin MPN model (Li et al., 2010) with a *Pbx1*-cKO mouse (Ficara et al., 2008). In the resulting



(legend on next page)



double-mutant JP mouse, the activation of the MPN-driver human heterozygous $JAK2^{V617F}$ mutation and PBX1 deletion are induced simultaneously by repeated pIpC injections (Figures 1A and 1B). Recombination was always verified at the first peripheral blood (PB) draw (and at necropsy on BM-derived colonies; see also Note S1 and Figure S2).

We followed the disease kinetics for several weeks in $JAK2$ -cKI and in JP mice, by comparing their blood parameters with those of our cohort of wild-type (WT) and $Pbx1$ -cKO control mice. Starting from 4 weeks after the last pIpC injection, PB was drawn at regular intervals and analyzed by hemocytometer, up to at least 40 weeks from Cre induction. $JAK2$ -cKI mice developed a mild but significant erythrocytosis in both male and female mice, with increased hematocrit, hemoglobin (HGB), and red blood cell counts compared with WT mice, as expected (Figures 1C and S3A). In JP mice, a similar increase in all these parameters was noted up to 12 weeks after pIpC (Figure 1C), despite conditional inactivation of PBX1 alone leading to anemia (Figure S3B). At later time points, however, erythrocytosis was progressively less evident in JP mice, reaching at week 16–20 hematological parameters similar to those of WT mice (Figure 1C). HGB values were even lower than those of WT mice at the latest time points, raising some concern regarding possible development of a mild form of hypochromic anemia in the long run, as suggested by analyzing median corpuscular hemoglobin (MCH) and MCH concentration (MCHC) values (Figure S3C). JP platelet counts, on the other hand, were similar to or lower than those of WT mice throughout the observation time,

including the earliest time points (Figures 1D and S3D), suggesting a prominent role of $Pbx1$ in platelet development or production, as suggested by the thrombocytopenia observed in $Pbx1$ -cKO mice (Figure S3E). The increase in granulocyte counts was also rescued, starting from the first observation times (Figure 1E, left; a representative blood smear is shown on the right), but only up to week 24 and week 8 in male or female mice, respectively (Figure S3F), whereas at later time points the high variability in all experimental groups hampered further evaluations. Overall, the absence of PBX1 rescued the alteration of blood parameters in $JAK2$ -cKI mice.

$JAK2$ -cKI and all control mice survived throughout all the observation time, including $Pbx1$ -cKO mice, despite their stem cell defect. Although features of MPN were abrogated in the absence of PBX1, some JP mice succumbed for unknown reasons, with signs of pancytopenia for some of them (Figure S4A). At necropsy, FACS analysis of BM and spleen showed that the proportion of lymphoid ($CD19^+$, $CD4^+$, $CD8^+$) and myeloid ($CD11b^+$) cells was similar in all mice (not shown). Histology data confirmed development of an MPN-like disease in $JAK2$ -cKI mice, which displayed myeloid metaplasia in the spleen, indicated by the presence of megakaryocytic hyperplasia and of excess of myeloid cells (Figure 1F), but not in JP mice or in control animals (Figures 1F and S4B). Quantification of the splenic megakaryocytes revealed a complete normalization of this phenotype in the absence of PBX1 (Figure 1F). Finally, colony assays performed with BM cells derived from mice revealed that the *in vitro* EPO independent burst forming unit-erythroid (BFU-E) growth typical of MPN cells from

Figure 1. Generation and analysis of the JP mouse model

(A) Crossing of $Mx1Cre^+.JAK2^{+/V617F}$ ($JAK2$ -cKI) with $Pbx1^{fl/fl}$ ($Pbx1$ -cKO) mice generated the double-mutant JP model $Mx1Cre^+.JAK2^{+/V617F}.Pbx1^{fl/fl}$. Diagram on the left shows the $JAK2^{V617F}$ knockin allele and the activated recombined allele after Cre-mediated excision of the PGK *Neo* cassette due to the presence of *LoxP* sites. On the right, *LoxP* sites surrounding exon 3 of $Pbx1$ allow the allele recombination resulting in $Pbx1$ inactivation.

(B) WT, $JAK2$ -cKI, or JP mice, 4–6 weeks old, were administered with pIpC. Starting 4 weeks from last injection, PB was analyzed periodically. At the end of the monitoring period, animals were sacrificed to analyze BM and spleen. $CD11b^+$ cells were purified from PB at the first blood withdrawal.

(C–E) Time course analysis of blood parameters in $JAK2$ -cKI, WT, and JP mice. Results from male and female mice were pooled, see Figure S3 for separate values. (C) Red blood cell (RBC) counts, hematocrit (HCT), and hemoglobin (HGB); (D) platelet (PLT) counts; (E) granulocyte (GRA) counts, with representative week 20 blood smear images on the right. Data are represented as mean \pm SEM ($n = 19$ –21 individual mice). For each plot, *wks* on x axis refers to weeks from the last pIpC injection. For each parameter, the entire trend of $JAK2$ -cKI and WT mice is significantly different; $p = 0.0001$ in (C) and (E), $p = 0.03$ in (D) (these statistics are not shown within the graph for simplicity). Asterisk (*) and hash (#) symbols within the graphs indicate p values for each time point. Asterisk refers to the comparison between JP and WT mice, hash to the comparison between JP and $JAK2$ -cKI mice. Images were acquired with an Olympus XC50 camera mounted on a BX51 microscope, using CellF Imaging software. Scale bar within the right panel refers to both images.

(F) Representative images of spleen histology (H&E staining) showing myeloid metaplasia with megakaryocytic hyperplasia in $JAK2$ -cKI mice. Quantification of megakaryocytes (number of Mk/area) is represented in the scatterplot; $n = 15$ –22 individual mice; Kruskal-Wallis test. Scale bar within the upper left panel refers to all three images.

(G) Scatterplot indicating the number of BFU-E generated from 2×10^5 total BM cells in the absence of EPO in the three mouse models; $n = 8$, 9, and 7 individual WT, $JAK2$ -cKI, and JP mice, respectively; ordinary one-way ANOVA test. In (F) and (G), bars indicate mean \pm SD. * and #, $p < 0.05$; ** and ##, $p < 0.01$; *** and ###, $p < 0.001$.

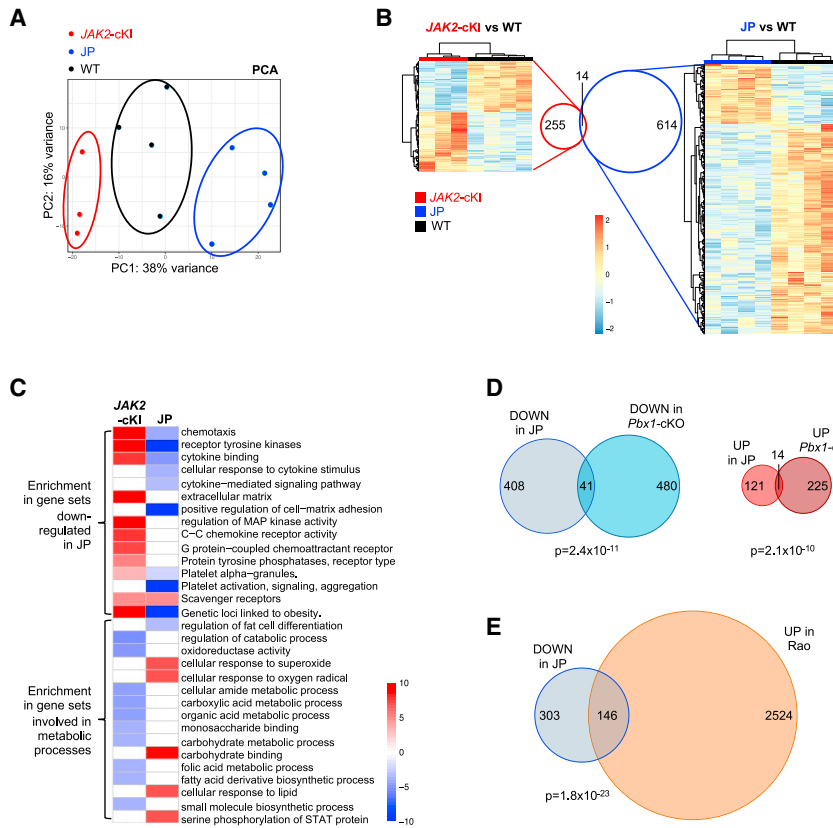


Figure 2. RNA-seq to discover molecular pathways deregulated in absence of PBX1 (A) PCA of *JAK2*-cKI, JP, and WT LKS (red, blue, and black, respectively).

(B) Hierarchical cluster dendrogram showing the relative expression of DE transcripts in *JAK2*-cKI LKS compared with WT (left) and in JP LKS compared with WT (right). Venn diagram shows the overlap of deregulated genes in the two analyses. The color scale represents Z score transformed signal intensity.

(C) Heatmap showing the enrichment score (minimum, -10 ; maximum, 10) from gene set enrichment analysis in the indicated categories for each gene set compared with WT.

(D) Venn diagrams showing overlaps among genes downregulated (left) and upregulated (right) in both JP and *Pbx1*-cKO HSPCs.

(E) Venn diagram showing overlap among genes downregulated in JP LKS and genes upregulated in MEP from VF mice, a transgenic MPN model with *Jak2*^{V617F} mutation described in Rao et al. (2019).

the *JAK2*-cKI mouse model (Li et al., 2010) was rescued in the absence of PBX1 (Figure 1G).

In conclusion, PBX1-dependant pathways control disease course for at least 40 weeks after the induction of the disease.

PBX1 controls molecular pathways deregulated by the *JAK2*^{V617F} mutation in HSPCs

To discover pathways deregulated by the *JAK2*^{V617F} mutation that are already affected by *Pbx1* at the level of HSPCs, we performed RNA-seq on FACS-sorted Lineage⁻/cKit⁺/Sca1⁺ (LKS) cells from the BM of individual WT, *JAK2*-cKI, and JP mice several weeks after induction of the *JAK2* mutation and/or PBX1 deletion. Transcriptional data on *Pbx1*-cKO control HSPCs were already available (Ficara et al., 2008) and are included in Table S1. LKS were chosen since they are enriched for HSCs (Figure S4C, top panels), but they also include committed progenitors, thus comprising the cell population(s) that most likely sustain the disease long term; the proportion of LKS within the BM was similar in the three groups of mice, as well as the proportion of HSCs within LKS (Figure S4C, bottom).

Principal component analysis (PCA) shows that LKS from *JAK2*-cKI, WT, and JP mice cluster separately (Figure 2A), indicating intra-group homogeneity and good sample reso-

lution among the three conditions. Differential expression analysis revealed that 269 and 628 genes were differentially expressed (DE) at false discovery rate <0.05 in *JAK2*-cKI and in JP mice compared with WT, respectively (Figure 2B and Table S2). There was only a minimal overlap between the two gene sets (Figure 2B), indicating that the expression level of the vast majority of the genes DE in MPN-affected mice compared with WT was rescued by the absence of PBX1, since they were no longer DE in JP mice compared with WT. Of the 14 common genes, nine changed discordantly in the two gene sets: four were upregulated in *JAK2*-cKI but downregulated in JP mice, mostly involved in vesicular trafficking, and five were downregulated in *JAK2*-cKI but upregulated in JP mice (Table S2).

Genes downregulated in LKS from *JAK2*-cKI mice compared with WT were enriched for several metabolic processes (Figure 2C, bottom). A misregulation of genes involved in metabolism in megakaryocyte-erythrocyte progenitors (MEPs) has been described (Rao et al., 2019), and we here show that similar alterations are already present at the level of uncommitted cells in *JAK2*-cKI, but not in JP mice. Genes upregulated in LKS from *JAK2*-cKI mice compared with WT were enriched for several gene families and pathways involved in MPN pathogenesis, including receptor tyrosine kinases, extracellular matrix, cytokine

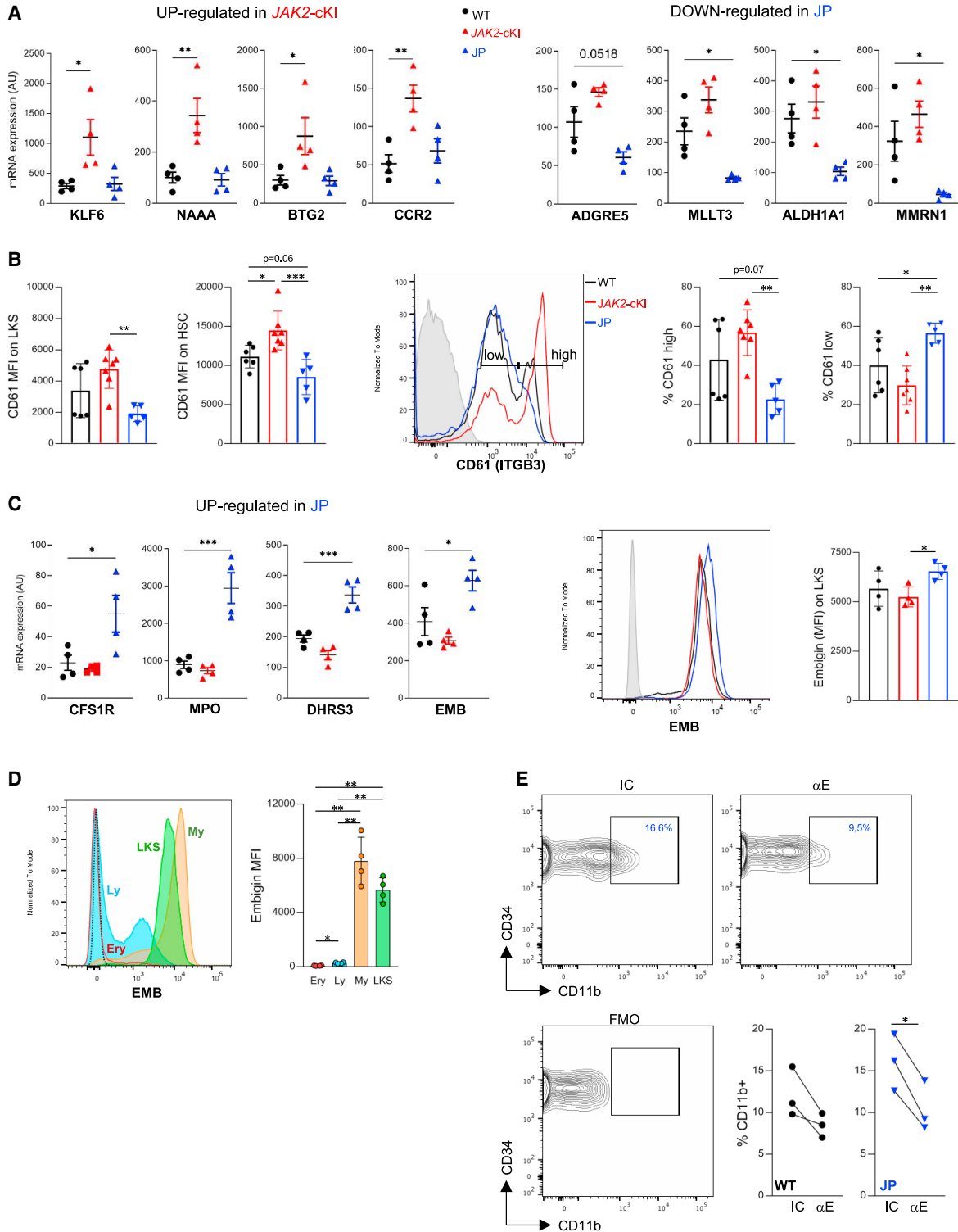


Figure 3. Validation of RNA-seq data

(A) Scatterplots showing real-time PCR data for the indicated genes expressed in arbitrary units (AU).

(B) FACS analysis showing CD61 expression in BM LKS and HSCs of pIpC-treated *JAK2-cKI*, JP, and WT mice. MFI, mean fluorescence intensity. Representative overlay histograms indicating CD61-high and -low gates are shown.

(legend continued on next page)



binding, platelet activation, and for previously published gene sets related to lipids. The same gene families and pathways were enriched in the list of genes downregulated in LKS from JP mice (Figure 2C, top), suggesting that their expression in LKS from MPN-affected mice is dependent on *Pbx1*.

Among genes DE in JP LKS compared with WT, we also found a significant overlap with the PBX1 signature (Figure 2D), indicating that at least part of the expression profile of the JP mice is the result of the absence of PBX1 per se, regardless of the JAK2 unregulated expression. Downregulated overlapping transcripts are mainly involved in calcium binding, HSC maintenance, cancer, and platelet development/function (Table S3), in line with our current experimental data; upregulated genes play roles in inflammation and in the innate immune system, as expected from *Pbx1*-cKO mice. However, most of the non-overlapping DE genes likely change their expression level as the result of the concomitant JAK2 constitutive expression and PBX1 absence. Of note, 32.5% of the genes downregulated in JP LKS (including *Pbx1*) are upregulated in MEP from a similar murine MPN model (Rao et al., 2019) (Figure 2E; Table S3), despite PBX1 not normally being expressed in MEP (Figure S4D), indicating that, by deleting *Pbx1* in HSCs constitutively expressing JAK2, a portion of the genes contributing to MPN acting in committed progenitors are already repressed in LKS. Sixteen percent of the overlapping genes are also overexpressed in human MPN (Table S3).

We validated part of RNA-seq data with real-time PCR or FACS analysis (Figures 3A–3C). We confirmed elevated expression of KLF6 (a transcriptional activator), of NAAA (involved in fatty acid metabolism), BTG2 (correlated to terminal differentiation), and CCR2 (a chemokine receptor) in JAK2-cKI LKS compared with WT (Figure 3A, left panels). Genes confirmed to be downregulated in JP LKS included MLLT3 and ALDH1A1 (HSC stemness), ADGRE5 (CD97, regulator of leukemia stem cell function), MMRN1, and ITGB3 (CD61, platelet function) (Figure 3A, right panels, and Figure 3B). Downregulation of CD61 was confirmed at the protein level on both LKS and HSCs (Figure 3B, left). FACS analysis revealed the presence of CD61 high- and CD61 low-expressing LKS cells (Figure 3B, right), with JP LKS showing a reduced proportion of the CD61-high fraction and a concomitant increase of the

CD61-low fraction compared with JAK2-cKI and WT mice. Among genes upregulated in JP versus WT LKS, we tested CFS1R (CD115), MPO, DHRS3 (all normally expressed in myeloid cells) and Embigin (EMB; a cell adhesion molecule), which we also confirmed at the protein level (Figure 3C). Interestingly, FACS analysis of WT BM cells revealed an expression pattern that suggests EMB as a novel myeloid differentiation marker (Figure 3D). EMB was recently included among HSC regulators since its expression in the BM microenvironment promotes HSC homing (Silberstein et al., 2016); however, its function within HSPCs has not been dissected out. To gain insight into EMB's role within early progenitors, we sorted LKS cells and incubated them with an anti-EMB (α E)-blocking antibody (Ab) (Silberstein et al., 2016) in short-term culture. After 3 days, the proportion of cells that had acquired the CD11b myeloid marker was lower in cells treated with the α E Ab compared with isotype control (Figure 3E), suggesting that EMB downregulation prevents myeloid differentiation and that its overexpression in JP LKS, together with CFS1R and MPO, likely favors the myeloid lineage at the expenses of erythroid and MK lineages.

In conclusion, despite the blood pathology in MPN being mediated by differentiated cells, several molecular pathways are already deregulated in HSPCs. Transcriptional profiling data suggest that most of them are directly or indirectly under the control of PBX1. Our lists of DE genes provide a tool to select new therapeutic targets.

DISCUSSION

In this study, we demonstrate an essential role for PBX1 in determining the course of JAK2^{V617F} MPN through the analysis of a mouse model of the disease. Our data indicate that, despite the mutation in JAK2, thrombocytosis and granulocytosis do not develop in the absence of PBX1, in accordance with the high level of expression of PBX1 in the progenitors of these lineages in normal conditions (Seita et al., 2012) and with the low number of platelets in *Pbx1*-cKO mice; importantly, we also show that erythrocytosis normalizes after a few weeks in JP mice. We confirm that PBX1 sustains the expression of transcriptional programs that control HSC maintenance and platelet development, and prevent myeloid skewing, all relevant for MPN

(C) Left: real-time PCR data for genes upregulated in JP mice. Right: EMB expression in BM LKS cells of JAK2-cKI, JP, and WT mice measured by FACS. (B–C) FACS histograms in gray: unstained control.

(D) EMB protein level in erythroid (Ery), lymphoid (Ly), myeloid (My) (all gated based on scatters), and LKS cells in the BM of WT mice; a representative FACS analysis is shown on the left (dotted line: unstained). (A–D) Ordinary one-way ANOVA.

(E) Percentage of cells expressing CD11b after 3 days of liquid culture of LKS cells treated with α E or isotype control (IC); representative FACS contour plots of a JP sample are shown; paired t test.

For all bar graphs, bars indicate mean \pm SD. *, $p < 0.05$; **, $p < 0.01$, ***, $p < 0.001$.



onset, and we show that, in combination with mutated *JAK2*, PBX1 contributes to regulate signaling and metabolic pathways that are key for MPN and that are already active in primitive progenitors.

Conditional inactivation of PBX1 alone led to anemia, likely due to the known PBX1 role in preserving HSC functions and erythroid potential. Nevertheless, this property does not affect disease development during the first weeks after pIpC injection, underlying the prominent role of *JAK2* signaling in promoting proliferation, survival, and differentiation of erythroid progenitors, despite PBX1 absence. However, our data suggest that, to fuel the disease, proper HSC functionality, including long-term self-renewal, must be maintained over time. Whether similar conclusions could be drawn by deleting other genes that maintain fitness of HSCs is worth investigating.

Since PBX1 must be expressed to sustain the disease, we propose that acting on PBX1, or on pathways downstream of it, might represent an option for a long-term cure of MPN, to complement the action of conventional therapies or of more recent treatments based on JAK inhibitors (Vanucchi and Harrison, 2017). Modulation of PBX1 activity by direct targeting or by targeting its downstream mediators might represent a novel therapeutic approach that likely hits MPN stem cells rather than the bulk of the disease. Small molecules targeting PBX1 have been developed and tested in cancer models (Morgan et al., 2012; Platais et al., 2018; Shen et al., 2018, 2019), and selective toxicity for neoplastic cells has been demonstrated *in vitro* (Liu et al., 2019); moreover, their therapeutic potential has been proposed for several types of tumors (Morgan et al., 2012). However, the high number of genes DE in JP LKS compared with WT, and the fact that some JP mice died likely of ineffective hematopoiesis, suggest some caution before considering PBX1 inhibition in patients. Our approach of genetic inactivation as a proof of principle is very different from a pharmacologic approach, which would include dosage studies and would likely not reach a total abrogation of PBX1 activity. However, we also encourage the development of alternative or complementary strategies that target some of the druggable genes and pathways described here that are subordinated to PBX1 in the presence of mutated *JAK2*. Moreover, whether PBX1 could represent a novel prognostic factor is worth investigating, with the aim of further stratifying these heterogeneous patients and personalizing their therapeutic approach.

EXPERIMENTAL PROCEDURES

Murine models

Mx1Cre⁺JAK2^{V617F} and *Mx1Cre⁺Pbx1^{fl/fl}* mice have been described (Crisafulli et al., 2019; Koss et al., 2012; Li et al., 2010); see also supplemental experimental procedures. Primers used for genotyping are listed in Table S4.

Induction of *JAK2^{V617F}* expression and *Pbx1* deletion

Three- to 6-week-old mice were treated with 10 mg/kg pIpC (high molecular weight, InvivoGen) by intraperitoneal injection (seven doses, every other day). A detailed description is provided in supplemental experimental procedures.

Histological and FACS analysis

A detailed description is provided in supplemental experimental procedures. Monoclonal antibodies are listed in Table S4.

Colony-forming unit assay

To evaluate erythropoietin (EPO) independency, colony-forming unit (CFU) assay was performed from BM cells using the CAMEO-4 Kit (Preferred Cell Systems) as previously described (Li et al., 2010), with and without 3 U/mL h-EPO (R&D). See also supplemental experimental procedures.

RNA-seq and bioinformatic analysis

Total RNA was extracted with Direct-zol RNA Microprep kit (Zymo Research) from 5×10^4 LKS sorted from the BM of pIpC-treated *JAK2*-cKI, JP, and WT control mice (3–4 biological replicates/group). A detailed description is provided in supplemental experimental procedures.

Statistics

For time course analysis of blood parameters, data were compared using ANOVA for repeated measures when considering the entire curve, or with one-way ANOVA with *post hoc* Tukey's multiple comparison test when comparing individual time points. For all other multiple comparisons, Kruskal-Wallis test with Dunn's multiple comparisons test was used if normality test was not passed, or ordinary one-way ANOVA if data followed a normal distribution. $p < 0.05$ was considered statistically significant (* and # $p < 0.05$, ** and ## $p < 0.01$, *** and ### $p < 0.001$, **** $p < 0.0001$). Analyses were performed with GraphPad Prism (GraphPad Software) or with Stata15 (StataCorp LLC).

Data and code availability

The accession number for the RNA-seq data reported in this paper is GEO: GSE153482.

SUPPLEMENTAL INFORMATION

Supplemental information can be found online at <https://doi.org/10.1016/j.stemcr.2021.09.016>.

AUTHOR CONTRIBUTIONS

S.M. and L.C. conducted experiments; acquired, analyzed, and interpreted data; and wrote the manuscript. E.F., F.S.C., and R.R. conducted experiments. M.U. and M.G.D.P. provided patient samples and interpreted data. P.U. conducted bioinformatics analysis. E.M. analyzed data. C.P. was responsible for the RNA-seq. F.F. designed and directed research, oversaw data analysis, and wrote the manuscript. P.V. and A.V. supervised research and edited the manuscript.



CONFLICT OF INTERESTS

The authors declare no competing interests.

ACKNOWLEDGMENTS

The authors would like to thank Prof. Tony Green from Wellcome-MRC Cambridge Stem Cell Institute, Cambridge, UK, for providing us with *JAK2^{+/V617F}* cryopreserved embryos; Dr. Tina Hamilton for technical advice; and Stefano Mantero, Dario Strina, Lucia Susani, Dr. Javier Cibella, and Dr. Erica Travaglini for technical assistance. F.F. was supported by AIRC-Fondazione Cariplo (TRIDEO 15882). M.G.D.P. was supported by AIRC Foundation (project # 22053). S.M. was the recipient of a fellowship from Fondazione Damiano per l'Ematologia. L.C. was recipient of a fellowship from Fondazione Nicola del Roscio.

Received: January 4, 2021

Revised: September 21, 2021

Accepted: September 22, 2021

Published: October 21, 2021

REFERENCES

- Akada, H., Akada, S., Hutchison, R.E., Sakamoto, K., Wagner, K.U., and Mohi, G. (2014). Critical role of Jak2 in the maintenance and function of adult hematopoietic stem cells. *Stem Cells* 32, 1878–1889.
- Berkofsky-Fessler, W., Buzzai, M., Kim, M.K., Fruchtman, S., Najfeld, V., Min, D.J., Costa, F.F., Bischof, J.M., Soares, M.B., McConnell, M.J., et al. (2010). Transcriptional profiling of polycythemia vera identifies gene expression patterns both dependent and independent from the action of *JAK2V617F*. *Clin. Cancer Res.* 16, 4339–4352.
- Crisafulli, L., Muggeo, S., Uva, P., Wang, Y., Iwasaki, M., Locatelli, S., Anselmo, A., Colombo, F.S., Carlo-Stella, C., Cleary, M.L., et al. (2019). MicroRNA-127-3p controls murine hematopoietic stem cell maintenance by limiting differentiation. *Haematologica* 104, 1744–1755.
- Ficara, F., Crisafulli, L., Lin, C., Iwasaki, M., Smith, K.S., Zammataro, L., and Cleary, M.L. (2013). *Pbx1* restrains myeloid maturation while preserving lymphoid potential in hematopoietic progenitors. *J. Cell Sci.* 126, 3181–3191.
- Ficara, F., Murphy, M.J., Lin, M., and Cleary, M.L. (2008). *Pbx1* regulates self-renewal of long-term hematopoietic stem cells by maintaining their quiescence. *Cell Stem Cell* 2, 484–496.
- Guglielmelli, P., Zini, R., Bogani, C., Salati, S., Pancrazzi, A., Bianchi, E., Mannelli, F., Ferrari, S., Le Bousse-Kerdiles, M.C., Bosi, A., et al. (2007). Molecular profiling of CD34+ cells in idiopathic myelofibrosis identifies a set of disease-associated genes and reveals the clinical significance of Wilms' tumor gene 1 (*WT1*). *Stem Cells* 25, 165–173.
- Jung, J.G., Shih, I.M., Park, J.T., Gerry, E., Kim, T.H., Ayhan, A., Handschuh, K., Davidson, B., Fader, A.N., Selleri, L., et al. (2016). Ovarian cancer chemoresistance relies on the stem cell reprogramming factor *PBX1*. *Cancer Res.* 76, 6351–6361.
- Koss, M., Bolze, A., Brendolan, A., Saggese, M., Capellini, T.D., Bojilova, E., Boisson, B., Prall, O.W., Elliott, D.A., Solloway, M., et al. (2012). Congenital asplenia in mice and humans with mutations in a *Pbx/Nkx2-5/p15* module. *Dev. Cell* 22, 913–926.
- Li, J., Spensberger, D., Ahn, J.S., Anand, S., Beer, P.A., Ghevaert, C., Chen, E., Forrai, A., Scott, L.M., Ferreira, R., et al. (2010). *JAK2 V617F* impairs hematopoietic stem cell function in a conditional knock-in mouse model of *JAK2 V617F*-positive essential thrombocythemia. *Blood* 116, 1528–1538.
- Liu, Y., Xu, X., Lin, P., He, Y., Zhang, Y., Cao, B., Zhang, Z., Sethi, G., Liu, J., Zhou, X., et al. (2019). Inhibition of the deubiquitinase *USP9x* induces pre-B cell homeobox 1 (*PBX1*) degradation and thereby stimulates prostate cancer cell apoptosis. *J. Biol. Chem.* 294, 4572–4582.
- Longobardi, E., Penkov, D., Mateos, D., De Florian, G., Torres, M., and Blasi, F. (2014). Biochemistry of the tale transcription factors *PREP*, *MEIS*, and *PBX* in vertebrates. *Dev. Dyn.* 243, 59–75.
- Mead, A.J., and Mullally, A. (2017). Myeloproliferative neoplasm stem cells. *Blood* 129, 1607–1616.
- Moens, C.B., and Selleri, L. (2006). Hox cofactors in vertebrate development. *Dev. Biol.* 291, 193–206.
- Morgan, R., Boxall, A., Harrington, K.J., Simpson, G.R., Gillett, C., Michael, A., and Pandha, H.S. (2012). Targeting the *HOX/PBX* dimer in breast cancer. *Breast Cancer Res. Treat.* 136, 389–398.
- Nangalia, J., and Green, A.R. (2017). Myeloproliferative neoplasms: from origins to outcomes. *Blood* 130, 2475–2483.
- Nourse, J., Mellentin, J.D., Galili, N., Wilkinson, J., Stanbridge, E., Smith, S.D., and Cleary, M.L. (1990). Chromosomal translocation t(1;19) results in synthesis of a homeobox fusion mRNA that codes for a potential chimeric transcription factor. *Cell* 60, 535–545.
- Platais, C., Radhakrishnan, R., Niklander Ebensperger, S., Morgan, R., Lambert, D.W., and Hunter, K.D. (2018). Targeting *HOX-PBX* interactions causes death in oral potentially malignant and squamous carcinoma cells but not normal oral keratinocytes. *BMC Cancer* 18, 723.
- Rampal, R., Al-Shahrour, F., Abdel-Wahab, O., Patel, J.P., Brunel, J.P., Mermel, C.H., Bass, A.J., Pretz, J., Ahn, J., Hricik, T., et al. (2014). Integrated genomic analysis illustrates the central role of *JAK-STAT* pathway activation in myeloproliferative neoplasm pathogenesis. *Blood* 123, e123–e133.
- Rao, T.N., Hansen, N., Hilfiker, J., Rai, S., Majewska, J.M., Lekovic, D., Gezer, D., Andina, N., Galli, S., Cassel, T., et al. (2019). *JAK2*-mutant hematopoietic cells display metabolic alterations that can be targeted to treat myeloproliferative neoplasms. *Blood* 134, 1832–1846.
- Rice, K.L., Lin, X., Wolniak, K., Ebert, B.L., Berkofsky-Fessler, W., Buzzai, M., Sun, Y., Xi, C., Elkin, P., Levine, R., et al. (2011). Analysis of genomic aberrations and gene expression profiling identifies novel lesions and pathways in myeloproliferative neoplasms. *Blood Cancer J.* 1, e40.
- Seita, J., Sahoo, D., Rossi, D.J., Bhattacharya, D., Serwold, T., Inlay, M.A., Ehrlich, L.I., Fathman, J.W., Dill, D.L., and Weissman, I.L. (2012). Gene Expression Commons: an open platform for absolute gene expression profiling. *PLoS One* 7, e40321.



- Shen, A.Y., Jung, J., Rahmanto, Y.S., Selleri, L., Shih, I.-M., Chuang, C.M., and Wang, T.-L. (2018). A novel small-molecule compound targeting PBX1-DNA interaction impedes cancer cell survival and carboplatin resistance. In Proceedings of the American Association for Cancer Research Annual Meeting 2018, 78 (AACR), Abstract nr: 1966.
- Shen, L.Y., Zhou, T., Du, Y.B., Shi, Q., and Chen, K.N. (2019). Targeting HOX/PBX dimer formation as a potential therapeutic option in esophageal squamous cell carcinoma. *Cancer Sci.* *110*, 1735–1745.
- Shepherd, M.S., Li, J., Wilson, N.K., Oedekoven, C.A., Li, J., Belmonte, M., Fink, J., Prick, J.C.M., Pask, D.C., Hamilton, T.L., et al. (2018). Single-cell approaches identify the molecular network driving malignant hematopoietic stem cell self-renewal. *Blood* *132*, 791–803.
- Silberstein, L., Goncalves, K.A., Kharchenko, P.V., Turcotte, R., Kfoury, Y., Mercier, F., Baryawno, N., Severe, N., Bachand, J., Spencer, J.A., et al. (2016). Proximity-based differential single-cell analysis of the niche to identify stem/progenitor cell regulators. *Cell Stem Cell* *19*, 530–543.
- Tefferi, A. (2016). Myeloproliferative neoplasms: a decade of discoveries and treatment advances. *Am. J. Hematol.* *91*, 50–58.
- Vannucchi, A.M., and Harrison, C.N. (2017). Emerging treatments for classical myeloproliferative neoplasms. *Blood* *129*, 693–703.
- Wei, X., Yu, L., and Li, Y. (2018). PBX1 promotes the cell proliferation via JAK2/STAT3 signaling in clear cell renal carcinoma. *Biochem. Biophys. Res. Commun.* *500*, 650–657.

Stem Cell Reports, Volume 16

Supplemental Information

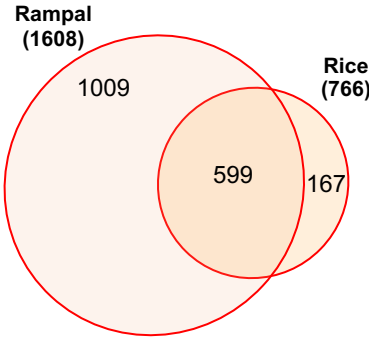
PBX1-directed stem cell transcriptional program drives tumor progression in myeloproliferative neoplasm

Sharon Muggeo, Laura Crisafulli, Paolo Uva, Elena Fontana, Marta Ubezio, Emanuela Morengi, Federico Simone Colombo, Rosita Rigoni, Clelia Peano, Paolo Vezzoni, Matteo Giovanni Della Porta, Anna Villa, and Francesca Ficara

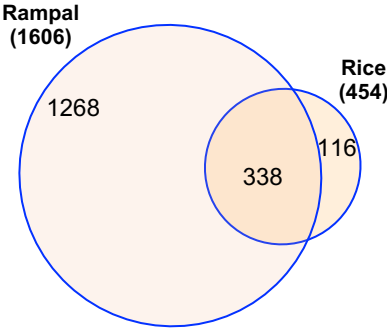
SUPPLEMENTAL FIGURES

Figure S1

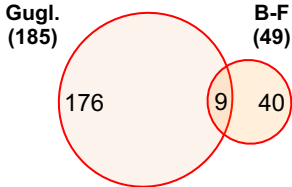
A Up-regulated (in granulocytes)



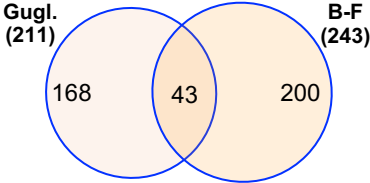
Down-regulated (in granulocytes)



B Up-regulated (in CD34+ cells)



Down-regulated (in CD34+ cells)



C

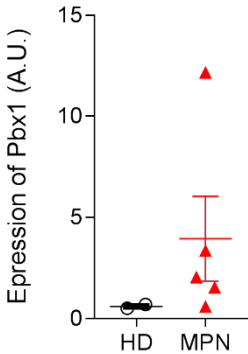
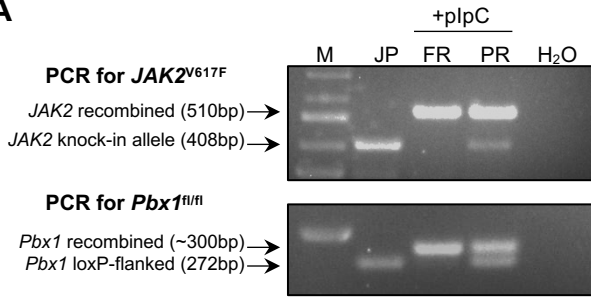


Figure S2

A



B

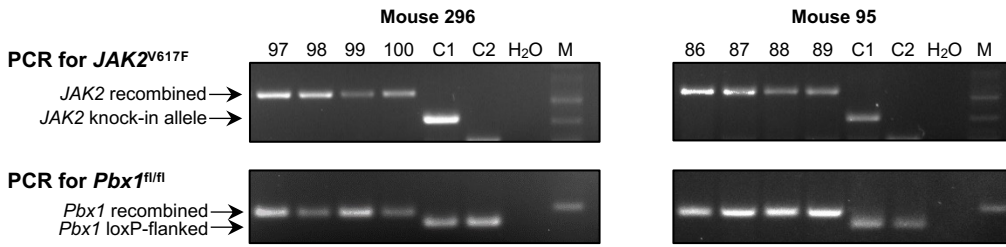
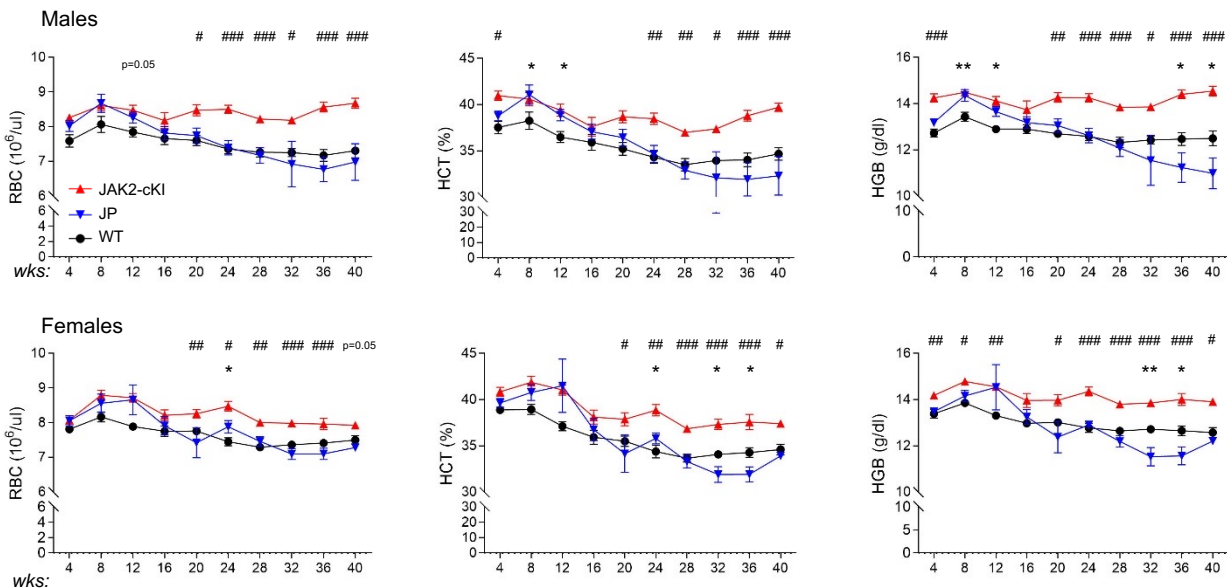
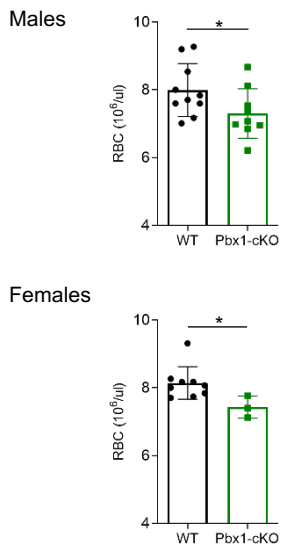


Figure S3

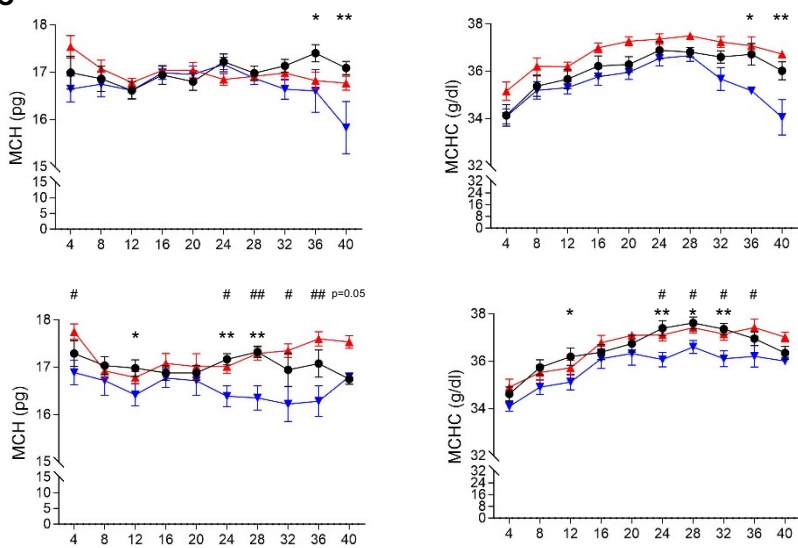
A



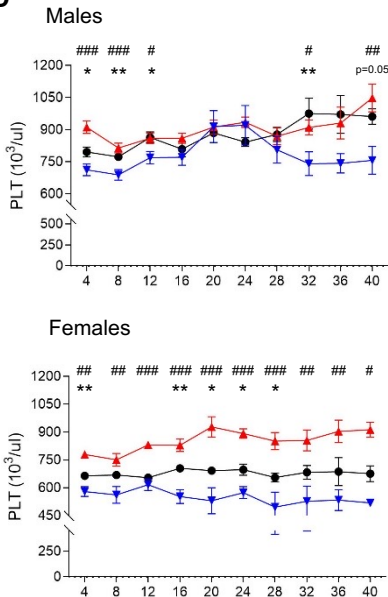
B



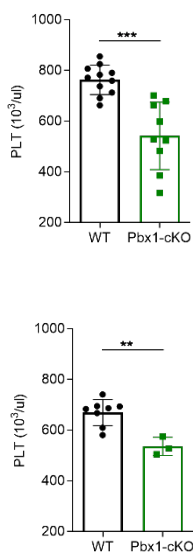
C



D



E



F

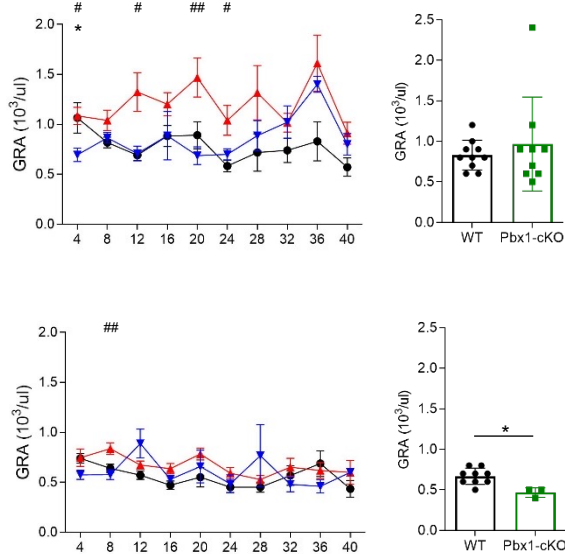
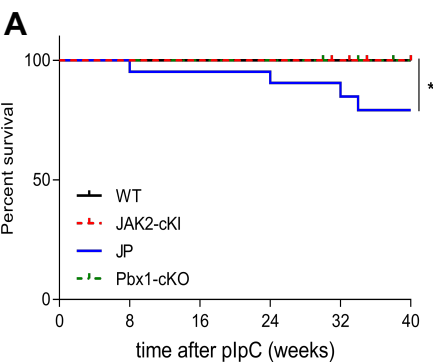
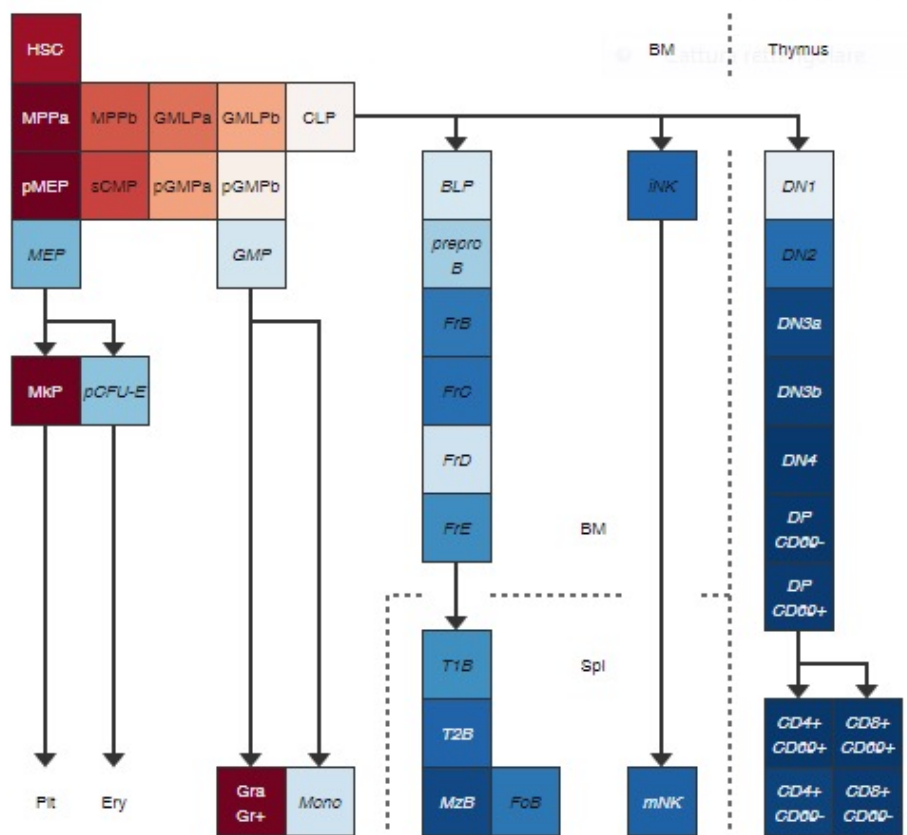
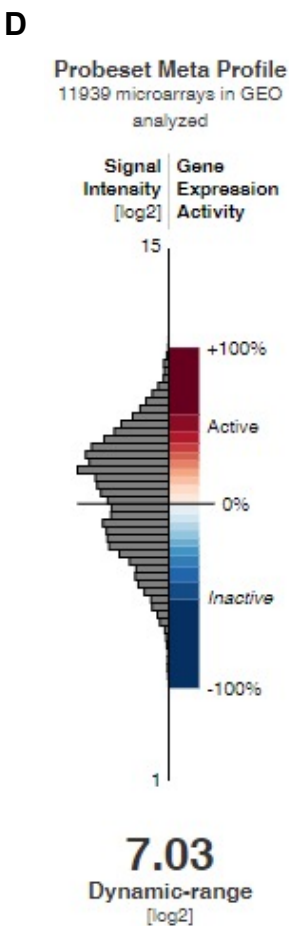
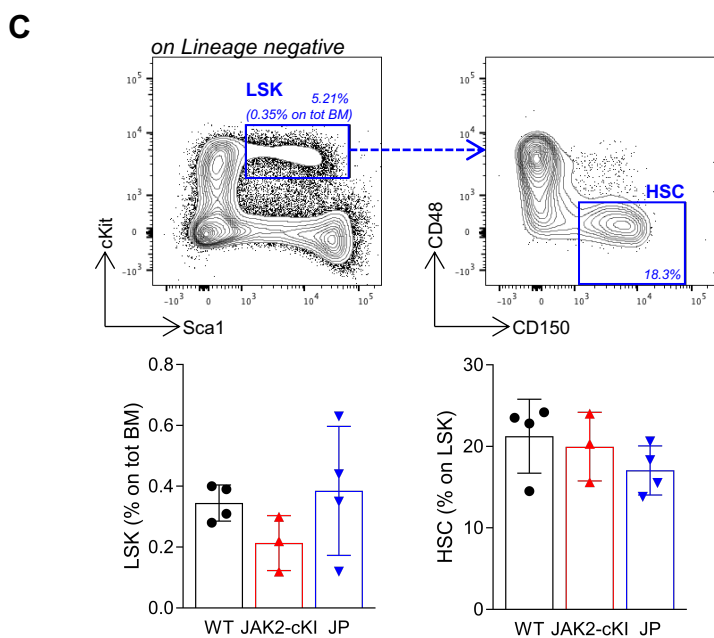
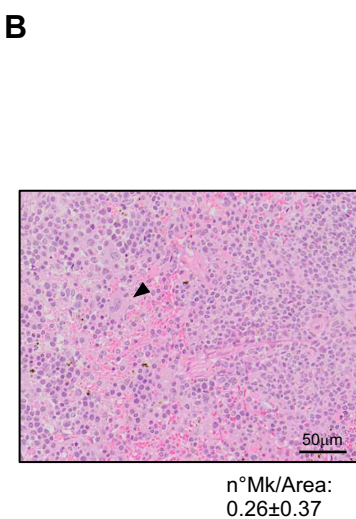


Figure S4



JP mice that did not survive

ID	Last PB	RBC (10 ⁶ /μl)	HCT (%)	HGB (g/dl)	PLT (10 ³ /μl)	GRA (10 ³ /μl)	MCH (pg)	MCHC (g/dl)
190	4wks	7.56	36.5	12.2	642	1.0	16.1	33.4
223	28wks	6.24	28.6	10.2	474	0.9	16.3	35.7
294	20wks	5.12	22.9	8.4	137	0.3	16.4	36.7
299	34wks	7.08	35.6	13.2	924	1.6	17.3	37.1



LEGENDS TO SUPPLEMENTAL FIGURES

Figure S1. PBX1 contribution in human MPN, Related to Table 1 and to the first paragraph of Results in the main text.

(A-B) Overlap between the MPN profiles retrieved from four previously published studies. (A) Up-regulated and down-regulated genes in the two studies performed using granulocytes from PV, ET and PMF patients. (B) Up-regulated and down-regulated genes in the two studies performed using CD34⁺ cells, from PV BM cells (B-F) or from PMF PB cells (Gugl.). The complete gene lists are included in Table S3. Gugl., Guglielmelli; B-F, Berkofsky-Fessler. In brackets the number of genes within each signature. (C) Expression of PBX1 in human MPN was measured by real-time PCR in CD34⁺ cells purified from the BM of healthy donors (HD, n=2) or of JAK2^{V617F} MPN patients (n=5: 3 ET, 2 PV). A.U., arbitrary units. For HD, bar indicate the range. Significance of the difference cannot be properly evaluated due to the limited size of the samples.

Figure S2. Allele recombination assessment, Related to the second paragraph of Results in the main-text and to note S1.

(A) Representative PCR analysis performed on CD11b⁺ cells to check for JAK2^{V617F} (top) and Pbx1^{fl/fl} (bottom) recombination. For both PCR the presence of a single band with a higher molecular weight compared to that obtained from untreated mice reveal full recombination (FR), while partial recombination (PR) is revealed by the presence of two bands. First lane: marker (M). Second lane: JP mouse prior to plpC induction (genotype screening). Third lane: complete Cre-mediated recombination after induction with plpC. Fourth lane: incomplete Cre-mediated recombination. Fifth lane: water. (B) Representative PCR analysis performed on individual HSC-derived colonies sorted from two JP mice (mouse 296 and mouse 95). For each gel picture: first four lanes: representative clones (4 out of 100 for both mice) showing FR of both JAK2^{V617F} and Pbx1^{fl/fl} in individual HSCs. Fifth lane (C1); control of the not recombined alleles (DNA of JP mouse prior to plpC induction). Sixth line (C2): WT control (for Pbx1-PCR, the not-recombined Pbx1^{fl/fl} allele and the wt allele produce a band with the same molecular weight). Seventh lane: water. Eighth lane: marker.

Figure S3. Additional analysis on blood parameters in all mice, Related to Figure 1.

(A) Time-course analysis of blood parameters relative to red blood cells in JAK2-cKI, WT and JP male (top) and female (bottom) mice. (B) RBC counts measured eight weeks after the last plpC injection in male (top) and female (bottom) Pbx1-cKO and WT mice. (C) Time-course analysis of additional blood parameters relative to red blood cells in JAK2-cKI, WT and JP male (top) and female (bottom) mice. (D) Time-course analysis of platelets concentration in JAK2-cKI, WT and JP male (top) and female (bottom) mice. (E) Platelets concentration measured eight weeks after the last plpC injection in male (top) and female (bottom) Pbx1-cKO and WT mice. p-value was calculated by applying a ttest, after performing Shapiro-Wilk normality test. (F) Left: time-course analysis of granulocytes concentration in JAK2-cKI, WT and JP male (top) and female (bottom) mice. Right: Granulocytes concentration measured eight weeks after the last plpC injection in male (top) and female (bottom) Pbx1-cKO and WT mice. For all time-course: see legend to Figure 1 for statistics.

Figure S4. Additional analysis on mice cohort and on RNA-Seq data, Related to Figures 1 and 2.

(A) Left: Kaplan-Mayer survival curves of the indicated mouse models (n=12-21; Log-rank test). Numbers on the x-axis indicate weeks from last plpC injection. Right: blood parameters of the four JP mice that succumbed before the experimental endpoint. Values refer to the analysis performed at the last time-point before death. (B) Representative image of spleen histology (H&E staining) and quantification of megakaryocytes ±SD (n=12) for Pbx1-cKO mice. The image was acquired with an Olympus Slide Scanner VS120-L100, with 20X magnification (50% reduction of a representative area is shown). (C) FACS analysis to detect stem and progenitor cells. Top panels: representative FACS analysis of JP BM cells. Contour plot on the left shows cells after Singlets/Live/Scatters/Lin⁻ gating; LKS cells were sorted for RNA-Seq. Contour plot on the right shows the percentage of HSC within the LKS gate. Bottom panels: the proportion of LKS within the BM was similar in the three groups of mice (scatter plot on the left), as well as the proportion of HSC within LKS.

(D) Schema of the mouse hematopoiesis model: the expression of PBX1 within 39 hematopoietic stem and progenitor populations in adult mouse BM, spleen, and thymus, retrieved from Gene Expression Commons, is shown.

SUPPLEMENTAL TABLES

Table S1. List of genes differentially expressed in hematopoietic stem and progenitor cell subsets from *Pbx1*-cKO mice, Related to Table 1 and Figure 2. Provided as Excel Spreadsheet.

Table S2. Genes DE in LKS from *JAK2*-cKI and from JP mice compared to WT, Related to Figures 2-3. Provided as Excel Spreadsheet.

Table S3. Result of the comparison among different gene sets, Related to Figure 2. Provided as Excel Spreadsheet.

Table S4. List of Reagents, Related to all figures.

Primers for genotyping or to assess recombination				
<i>Pbx1</i> WT/floxed (genotype)	KO5: GAG TTT GTC AGA GGA TTT TGT AGA TCT C KO6: CAC GTA CAA ATT GAG TTG ATA CAG TGG G			
<i>Pbx1</i> WT or floxed/recombined (recombination control)	KO1: TGA GTA TTC GGG GAG CCC AAG AA KO2: CAT GAT GCC CAG TCT GTA GGG GT KO5.5: GAG TTT GTC AGA GGA TTT TGT A KO8: GAC ATT CTT ATA GAA CCC GAG			
<i>JAK2</i> KI recombined (genotype and recombination control)	P1: TGT AAT CGA TCT GTC CTG AAT CGT GTA TGCT P4: TGG CTG GAC GTA AAC TCC TC P2: CCC TCC ATT TCT GTC ATC GT			
Antibodies[§]				
	CLONE	FLUOROCHROME	SUPPLIER*	CAT no.
mCD48	HM48.1	PE-Cy7; BV480	eBioscience™; BD Pharmingen™	25-0481-80; 746545
mCD117 (cKit)	2B8	BV786	BD Pharmingen™	564012
mCD150	TC15-12F12.2	APC	BioLegend	115910
mLy-6A/E (Sca-1)	D7	BV711; BV421; PE	BD Pharmingen™	563992; 562729
mCD34	RAM34	FITC	eBioscience™	11-0341-85
Lineage cocktail: CD3, B220, CD19, TER-119, CD11b, Gr-1	145-2C11; RA3-6B2; 1D3; TER-119; M1/70; RB6-8C5	PerCP-Cy5.5	eBioscience™	45-0031-82; 45-0452-82; 45-0193-82; 45-5921-82; 45-0112-82; 45-5931-80
mCD11b	M1/70	PerCP-Cy5.5; APC-eFluor 780	eBioscience™	45-0112-82 47-0112-82
hCD34	581	PE	BD Pharmingen™	560941
mCD61	2C9.G2	PE-Vio770	Miltenyi Biotec	130-102-627
mEMB	G7.43.1	PE; Purified**	eBioscience™	12-5839-80; 14-5839-85
Isotype control**	eB149/10H5	Purified	eBioscience™	14-4031-85
Primers for real-time PCR				
m_KLF6	FW	ACG AAA AGC TCC CAC TTG AA		
	REV	ACA ACC TTC CCA TGA GCA TC		
m_NAAA	FW	GCA TCT GTG ACT CGC TCA AC		
	REV	GGC CAC AAT ACT GGT GCA G		
m_CCR2	FW	TTG GCC ATC TCT GAC CTG CT		
	REV	GTG AGC CCA GAA TGG TAA TGT G		

m_BTG2	FW	GCG AGC AGA GAC TCA AGG TT
	REV	CCA GTG GTG TTT GTA ATG ATC G
m_DHRS3	FW	CAA AGC TGT CCG AGA GAA GG
	REV	TTT TTC CAT GGA CCA CAG C
m_MPO	FW	GAT GGA ATG GGG AGA AGC TC
	REV	GCA GGT AGT CCC GGT ATG TG
m_EMB	FW	GCC ATA CTT GCC GAA GTC A
	REV	TTC AAA TTC TTT CCC AGC ATC
m_MMM1	FW	TCA GCA GCA GAA GCA AGA CT
	REV	TTC CTC TCC TGT TGG CTC AG
m_MLLT3	FW	TGA CAA TGA CTC GGA GAT GG
	REV	CAC TGT CAC TGC CGT CAC TC
m_ALDH1A1	FW	GCC ATC ACT GTG TCA TCT GC
	REV	CAT CTT GAA TCC ACC GAA GG
m_ADGRE5	FW	ATC CAG CCA CGG TCA ACT AC
	REV	TTG TTG GGT TTC AGT CTC CAT
m_CSF1R	FW	CAG CAA TGA TGT TGG CAC A
	REV	TCA AGT TTA AGT AGG CAC TCT CCA
m_Actinb	FW	CTA AGG CCA ACC GTG AAA AG
	REV	ACC AGA GGC ATA CAG GGA C

§List of antibodies used for FACS analysis, for sorting and for cultures. *SUPPLIERS: eBioscience™: Thermo Fisher Scientific, Waltham, MA USA; BioLegend: San Diego, CA, USA; BD Pharmingen™: BD Bioscience, San Jose, CA, USA; Miltenyi Biotec: Bergisch Gladbach, North Rhine-Westphalia, Germany. **related to Figure 3E.

SUPPLEMENTAL NOTES

Note S1. Efficient gene deletion upon plpC repeated injections

Since plpC-induced Cre-mediated recombination might not occur in all cells, potentially affecting results due to the *in vivo* strong selective advantage of the very few *Pbx1*-not deleted cells, we set up a PCR strategy to assess the correct recombination process; we also performed pilot experiments to establish the optimal number of injections to obtain recombination in all HSPCs. JP mice were treated with 10mg/Kg of plpC for a total of four to seven injections performed every other day. After four weeks of washout period from the last administration, myeloid CD11b⁺ cells were isolated from the peripheral blood (PB), and PCR analysis was performed to check for the presence of residual LoxP-flanked alleles. Myeloid cells were chosen because, due to their high turnover rate, they are continuously produced by HSC and progenitors. For this reason, *Pbx1* deletion in CD11b⁺ cells is an indirect measure of its deletion in HSC. We assessed that with a seven-plpC injections regimen complete *Pbx1* deletion, indicated by the complete absence of the band corresponding to the loxP-flanked allele (see Figure S2A) was obtained most of the times. Thus, we adopted this protocol for all subsequent experiments. We also monitored recombination level of the mutated *JAK2* allele using, on the isolated CD11b⁺ cells, the same PCR protocol employed for genotyping (Figure S2A). Fewer than 10% of the animal had to be excluded due to incomplete recombination, indicated by the presence of a residual band corresponding to the loxP-flanked allele. Recombination was also confirmed at sacrifice on DNA extracted from the pool of BM derived colonies using the same PCR strategy. Importantly, we were able to demonstrate recombination of both *JAK2* and *Pbx1* on individual HSCs (Figure S2B). We sorted HSCs from the BM of two JP mice >40 weeks after the last plpC injection and performed a clonogenic CFC assays. Individual colonies, derived from single HSCs, were picked, DNA was extracted, and PCR performed to ascertain that recombination of both alleles occurred within the same HSC. For both mice all the screened colonies revealed complete recombination in both alleles.

With respect to the original paper describing the *JAK2*-cKI model (Li et al., 2010), we observed a slightly different phenotype, with prevalence of erythrocytosis over thrombocytosis (see Figure 1). This might be due to the different animal facility and to the rederivation procedure. However, it should be noted that in the original publication a protocol of three plpC injections was used to induce the V617F mutation in *JAK2*, with recombination occurring in a portion of the cells, whereas with our seven injections protocol we routinely obtained complete recombination. This might result in different allele burden, potentially justifying the observed differences. Indeed, heterogeneity of MPN phenotype in patients is known to be influenced by the level of mutant *JAK2* signaling (Nangalia and Green, 2017). After the mutation event in heterozygosity, uniparental

disomy might occur, due to a mitotic recombination with duplication of the mutant allele. The prevalence of cells homozygous for the mutation increases with time, due to a proliferative or survival advantage; in patients a double dose of V617F favors erythrocytosis at the expenses of thrombocytosis for reasons that are not completely understood. However, the quoted differences did not affect the evaluation of Pbx1 role in MPN.

SUPPLEMENTAL EXPERIMENTAL PROCEDURES

Murine models

Animals were housed and bred in the specific-pathogen-free animal facility at Humanitas Research Hospital. All experimental procedures were performed with the approval of and in accordance with Humanitas Research Hospital's Administrative Panel on Laboratory Animal Care, in compliance with Italian and international law and policies. The study was approved by the Italian Ministry of Health (approval no. 444-2017-PR).

Briefly, *JAK2^{+V617F}* mice obtained from cryopreserved embryos, kindly provided by Dr. AR Green (Wellcome-MRC Cambridge Stem Cell Institute, Cambridge, UK), were crossed to *Mx1Cre⁺* mice to obtain the described *JAK2*-cKI MPN model (Li et al., 2010). *JAK2*-cKI mice were then bred to *Pbx1^{fl/fl}* mice to generate the final JP model with the *Mx1Cre⁺.Pbx1^{fl/fl}.JAK2^{+V617F}* genotype. All animals were on a C57BL/6J background. Mice were genotyped by polymerase chain reaction (PCR) (DNA Polymerase BIOTOOLS) using DNA extracted from ear biopsies. Primers are listed in Table S4. Control mice were littermate *Mx1Cre⁻.Pbx1^{fl/fl}* or *WT* (*Mx1Cre⁻.Pbx1^{+/+}.JAK2^{+/+}*), all designated as "WT" for simplicity. No differences were noted between *Mx1Cre⁻.Pbx1^{fl/fl}*, *Mx1Cre⁺.Pbx1^{+/+}* or *WT* mice.

Induction of JAK2V617F expression and Pbx1 deletion

Three to six-week-old mice were treated with 10mg/Kg plpC (High Molecular Weight, InvivoGen) by intraperitoneal injection (7 doses, every other day). Four weeks after the last plpC administration, peripheral blood (PB) was drawn from isoflurane-anesthetized mice (XGI-8 or RC2+ rodent gas anesthesia systems, Caliper Life Sciences, and VisEn Medical's, respectively) by retro-orbital bleeding with a heparinized capillary (VWR Hirschmann) and collected in ethylenediaminetetraacetic acid dipotassium salt (K2EDTA) spray coated microtainer (BD). Fresh whole blood was analyzed using Mythic18 VET Hemocytometer (Orphée). Blood smears were prepared and stained with MayGrunwald-Giemsa (Merck-Sigma Aldrich). Hemocytometer analysis and blood smears were repeated every four weeks.

LoxP recombination control

CD11b⁺ cells were immunomagnetically purified from the first PB draw using mouse CD11b⁺ MicroBeads Kit and the AutoMACS Pro cell separator (both Miltenyi Biotec), according to the manufacturer instructions. Purity was assessed by flow cytometry. DNA was extracted and PCRs were performed with the primers listed in Table S4. Recombination was also confirmed at sacrifice on DNA extracted from BM derived colonies using the same PCR strategy. Mice with incomplete recombination were excluded from the analysis.

Histological analysis

Spleens (half organ) were fixed in 4% formalin, dehydrated and paraffin embedded; sections (1.5 μm) were performed for classic hematoxylin and eosin (H&E) staining (Histo-Line) to check for basic histopathological changes/features. Images of sections was performed by Olympus Slide Scanner VS120-L100 (Olympus Optical Co.). Quantification of megakaryocytes (Mk) was manually performed on all spleen sections and normalized to the section area (cell number/mm²) using ImageJ software (<https://imagej.nih.gov/ij/>).

Flow Cytometry

BM cells were harvested by crushing of multiple bones (femurs, tibias, humeri, ulnae, sternum, hips). Splenocyte suspension was obtained by mechanical smashing of freshly isolated spleen (half organ) on a 40μm filter followed by red blood cells (RBC) lysis. Dead cell discrimination was performed with LIVE/DEAD Fixable Aqua Dead Cell Stain Kit (ThermoFisher Scientific), following manufacturer instructions. Cell staining was performed in PBS pH 7.2, 2% FBS, 1mM EDTA for FACS analysis or PBS pH 7.2, 0.5% BSA, 2mM EDTA for cell sorting. BM LKS and splenic HSC (LKS/CD48⁻/CD150⁺/Flk2⁻) were identified using the fluorochrome-conjugated monoclonal antibodies listed in Table S4. Data were acquired using LSR Fortessa (BD Bioscience). Cell sortings were performed using FACSAria III (BD Biosciences). All instruments were equipped with BD FACSDIVA software (BD), and data were analyzed using FlowJo (Tree Star, BD).

Colony Forming Unit assay

BM derived colonies w/o EPO were scored at day 9 before and after the 1-Step Ultra TMB-ELISA Substrate Solution (ThermoFisher Scientific) specific red-colony colorimetric assay (Reynolds et al., 1981). To verify

LoxP site recombination BM cells were seeded into methylcellulose-based medium (MethoCult GF M3434; StemCell Technologies) in duplicate in 35mm dishes. Colonies were pooled at day 10 and recombination was assessed by PCR on cell lysates.

Liquid Culture

LKS were FACS-purified from the BM of plpC-treated JP or WT mice, and cultured in U-bottomed tissue-culture treated wells in 200 μ l of serum free StemSpan medium (Stem Cell Technologies) supplemented with 100 ng/ml murine stem cell factor, 50 ng/ml murine thrombopoietin, 20 ng/ml human FLT-3 Ligand and of murine interleukin 3 (all Peprotech) (4000 cells/well). LKS cells from each individual mouse were split in two conditions: one supplemented with α E Ab, and the other with the isotype control (both at 2 μ g/mL). Both antibodies were freshly replaced every day.

RNA-Sequencing and bioinformatic analysis

The quality of total RNAs was evaluated with the TapeStation 4200 Agilent (Agilent); only RNAs having a RIN>8 were used for library preparations. Libraries for Poly(A) mRNA sequencing were constructed using the SMART-Seq v4 Ultra Low Input RNA kit (Takara Clontech) according to manufacturer's instruction. Sequencing was performed with the NextSeq 500 (Illumina). All libraries were sequenced in single-end mode (75bp length). On average, 25x10⁶ 75bp-long single-end reads were generated for each sample, with %Q30=89.46. Sequences were analyzed with Kallisto (Bray et al., 2016) and further processed with DESeq2 (Love et al., 2014) R package for differential expression analysis. Differentially expressed (DE) genes were determined considering False Discovery Rate (FDR) corrected p-values (FDR <0.05). Principle component analysis (PCA) was carried out on all genes analyzed. Enrichment analysis using DE genes were computed using ToppCluster software (<https://toppcluster.cchmc.org/help/>) (Chen et al., 2007). For the analysis of the overlap, Fisher's exact test p value was calculated with GeneOverlap R package.

Human samples

Approval of human studies by the IRCCS Humanitas Research Hospital Institutional Ethical Committee was obtained (prot. n. CE Humanitas, as per Ministerial Decree 8/2/2013, #29/18). Written informed consent was received from patients prior to inclusion in the study.

BM mononuclear cells were obtained from patients affected by MPN by density gradient centrifugation (Lympholyte-H Cell Separation, CEDARLANE). CD34⁻ cells were obtained by immunomagnetic depletion of CD34⁺ cells using mouse CD34 MicroBead Kit (Miltenyi Biotec) and AutoMACS Pro cell separator (Miltenyi Biotec), according to the manufacturer instructions. Purity was assessed by flow cytometry. CD34⁻ cells were stored in RNAlater (Merck-Sigma Aldrich).

Gene expression analysis

For PBX1 expression: RNA was extracted from CD34⁻ cells using QIAzol Lysis Reagent (Qiagen) and retrotranscribed using High-Capacity cDNA Reverse Transcription Kit (Thermo Fisher Scientific). PBX1 expression level was measured by real-time PCR using TaqMan Gene Expression Assay (Applied Biosystems, ThermoFisher Scientific; AssayID: Hs00231228_m1). Reactions were performed in duplicate using QuantStudio5 (Thermo Fisher Scientific). PBX1 expression level was normalized to ACTB (Applied Biosystems, ThermoFisher Scientific; AssayID: Hs01060665_g1). The relative amounts of mRNAs were calculated as 2^{- Δ CT} and expressed as arbitrary units.

For validation of RNAseq data: RNA from BM-sorted LKS of plpC-treated JAK2-cKI, JP and WT mice was extracted using Direct-zol RNA MicroPrep kit (Zymo Research), retrotranscribed with iScriptTM Reverse Transcription Supermix (Biorad) and pre-amplified using SsoAdvancedTM PreAmp Supermix (Biorad). Gene expression of selected genes indicated in Figure 3 were quantified by real-time PCR using SsoAdvanced Universal SYBR[®] Green Supermix. Actin beta was used as housekeeping gene and the relative amounts of mRNAs were calculated as 2^{- Δ CT} and expressed as arbitrary units. Complete list of real time-PCR primers is reported in Table S4.

Validation experiments include both existing and new independent samples.

SUPPLEMENTAL REFERENCES

Bray, N.L., Pimentel, H., Melsted, P., and Pachter, L. (2016). Near-optimal probabilistic RNA-seq quantification. *Nature biotechnology* 34, 525-527.

Chen, J., Xu, H., Aronow, B.J., and Jegga, A.G. (2007). Improved human disease candidate gene prioritization using mouse phenotype. *BMC bioinformatics* 8, 392.

Love, M.I., Huber, W., and Anders, S. (2014). Moderated estimation of fold change and dispersion for RNA-seq data with DESeq2. *Genome biology* 15, 550.

Reynolds, M., Lawlor, E., McCann, S.R., and Temperley, I.J. (1981). Use of 3,3',5,5'-tetramethylbenzidine (TMB) in the identification of erythroid colonies. *Journal of clinical pathology* 34, 448-449.